# LANGMUIR

pubs.acs.org/Langmuir Article

# Direct Determination of Plasmon Enhancement Factor and Penetration Depths in Surface Enhanced IR Absorption Spectroscopy

Cindy Tseng, Anuj K. Pennathur, Drew Blauth, Noemi Salazar, and Jahan M. Dawlaty\*



Cite This: Langmuir 2023, 39, 3179-3184



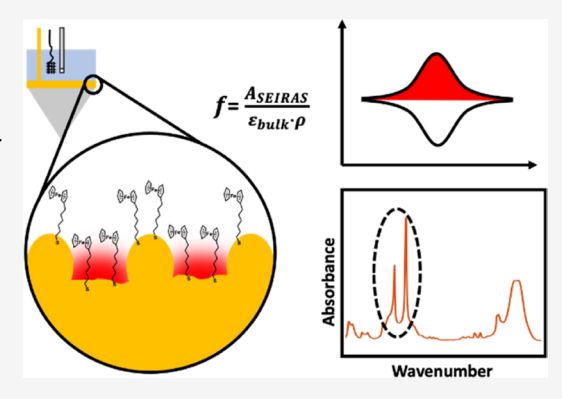
**ACCESS** I

III Metrics & More

Article Recommendations

Supporting Information

**ABSTRACT:** Surface Enhanced Infrared Absorption Spectroscopy (SEIRAS) is a powerful tool for studying a wide range of surface and electrochemical phenomena. For most electrochemical experiments the evanescent field of an IR beam partially penetrates through a thin metal electrode deposited on top of an attenuated total reflection (ATR) crystal to interact with molecules of interest. Despite its success, a major problem that complicates quantitative interpretation of the spectra from this method is the ambiguity of the enhancement factor due to plasmon effects in metals. We developed a systematic method for measuring this, which relies upon independent determination of surface coverage by Coulometry of a surface-bound redoxactive species. Following that, we measure the SEIRAS spectrum of the surface bound species, and from the knowledge of surface coverage, retrieve the effective molar absorptivity,  $\varepsilon_{\rm SEIRAS}$ . Comparing this to the independently



determined bulk molar absorptivity leads us to the enhancement factor  $f = \varepsilon_{\text{SEIRAS}}/\varepsilon_{\text{bulk}}$ . We report enhancement factors in excess of 1000 for the C–H stretches of surface bound ferrocene molecules. We additionally developed a methodical approach to measure the penetration depth of the evanescent field from the metal electrode into a thin film. Such systematic measure of the enhancement factor and penetration depth will help SEIRAS advance from a qualitative to a more quantitative method.

#### **■ INTRODUCTION**

Since its development in the 1980s, 1 Surface Enhanced IR Absorption Spectroscopy (SEIRAS) has opened several avenues to study spectroelectrochemical processes at interfaces. SEIRAS is an excellent tool for probing surface species in various electrochemical processes such as CO<sub>2</sub> reduction, <sup>2-10</sup> alcohol oxidation, <sup>11-13</sup> hydrogen evolution, <sup>14-16</sup> and water structure at surfaces. <sup>17-20</sup> In a nutshell, SEIRAS involves depositing a thin layer of metal on a substrate through which IR light can partially penetrate and interact with molecules. Unlike surface plasmon resonance (SPR) spectroscopy, exact momentum matching is not required for SEIRAS due to surface roughness. SEIRAS is often performed in an attenuated total reflection (ATR) geometry where the metal is directly deposited on top of the ATR crystal. Without the deposited metal layer, the theory to describe ATR is well developed, especially if the dielectric constant of the medium above the crystal is known.<sup>21,22</sup> However, for electrochemical measurements, metal deposition is necessary for electrical contact, which complicates the theory of ATR-SEIRAS.

Two phenomena emerge as a result of the metal deposition. First is the enhancement arising from interaction of the IR with the roughened metal and thereby producing an antenna effect that effectively increases the absorption cross section of the near-surface species.<sup>23</sup> Second, after metal deposition, the

penetration depth of the IR as understood from the dielectric theory of ATR no longer applies. In fact, if the metal is very thick, no light can interact with the near-surface molecules. Previously, the enhancement factor has been estimated by comparing absorption cross sections for the two scenarios — with and without roughened metal. <sup>23–25</sup> This, unfortunately, is not conclusive since the penetration depth is affected by the metal. Enhancement factor of SEIRAS, which fall in the range of 10–10,000, have been reported previously. <sup>25–30</sup> Lack of quantitative information for the enhancement factor makes interpretation of some experiments difficult and limits the utility of the technique. To resolve this issue, we report a systematic method for measuring the enhancement factor for SEIRAS of monolayers.

This paper is arranged as follows. First, we describe a method of determining the surface coverage of a monolayer on a SEIRAS substrate. Second, we measure the bulk molar absorptivity for certain vibrational features of our monolayer

Received: August 19, 2022 Revised: January 29, 2023 Published: February 22, 2023





sample. Third, we show SEIRAS spectra for the monolayer and, from their comparison to bulk spectra, extract the enhancement factor. Lastly, we show a quantitative method to determine the penetration depth of the IR beam from the metal substrate into a thin film.

#### EXPERIMENTAL SECTION

Gold was deposited on  $60^{\circ}$  cut ZnSe ATR prisms (Pike Technologies) via an electroless deposition method adapted from Bao et al. In summary, the ZnSe prism is heated on a hot plate at  $100~^{\circ}$ C, and is then exposed to a 10~mM HAuCl<sub>4</sub> solution for  $\sim 30~\text{s}$ . Prior to metal deposition, the ZnSe substrates were polished with alumina slurry (30, 15, 1, 0.05  $\mu$ m, consecutively) and then cleaned in an ultrasonic bath with ultrapure water for 5–10 min. This method produces a rough morphology as seen in the Scanning Electron Microscopy images reported. The gold thicknesses obtained from this method are in the order of 30 nm, as reported previously based on AFM measurements. The exact determination of the gold thickness is not a critical part of our analysis and outside the scope of this work, but it is estimated to be also of the same order.

Self-assembled monolayers (SAMs) were prepared by immersing the gold deposited ZnSe crystals in a 20 mM solution of 6-ferrocenyl hexanethiol (6-FCHT) in ethanol for 15–30 min to establish a dilute monolayer. The cyclic voltammograms for the SAMs were measured using a potentiostat (Gamry 1010B) from 0 to +0.6 V vs Ag/AgCl. The linear dependence of peak current versus scan rate establishes that the 6-FCHT was chemisorbed to the gold (see SI Figure S1). The working and counter electrodes were the deposited gold contacted with a gold wire (99.9% pure) and a Pt mesh, respectively. Prior to electrochemical measurements, both the gold wire and the Pt mesh were flame annealed, cleaned in piranha solution, and sonicated in ultrapure water. The electrolyte was 1 M KCl in aqueous solution.

Each ferrocene molecule undergoes one electron transfer in these potential regions, which allows calculation of surface coverage. The coverage of the monolayer was calculated by integrating the area under the curve of the anodic wave of the cyclic voltammogram. Prior to integration, the influence of the substrate's capacitive current from the voltammograms were baseline subtracted to extract the Faradaic current from the surface-bound ferrocenes, as explained in detail in the SI Figure S2. The geometric area of the electrode was 3.14 cm<sup>2</sup>.

The films of Prussian Blue (PB) were electrochemically deposited using methods followed by Roig et al. The ZnSe gold substrate working electrode was held at a constant cathodic current ( $-40~\mu A$ ) immersed in a 0.02 M in K<sub>3</sub>Fe(CN)<sub>6</sub>, 0.02 M FeCl<sub>3</sub>, 0.01 M HCl solution. Each  $\sim$ 14 nm layer was deposited by applying the current for 145 s, followed by taking a SEIRAS spectrum.

All spectra were collected using a ThermoFisher Nicolet iS50 FTIR spectrometer and a spectroelectrochemical Teflon cell that is compatible with the VeeMAX III (Pike Technologies) in the ATR geometry. The spectra were averaged for 128 scans with a resolution of 4 cm<sup>-1</sup>. The 6-FCHT monolayer SEIRAS spectra and PB film spectra were collected with a liquid nitrogen-cooled mercury cadmium telluride (MCT) detector and the bulk transmission FTIR spectra were collected with a deuterated tri-glycine sulfate (DTGS) room temperature detector. For bulk measurements, the molecules were dissolved in deuterated DMSO (dDMSO) to avoid overlap with the C-H stretch region of 6-FCHT. A CaF<sub>2</sub> FTIR cell with a 100  $\mu$ m spacer was used for the bulk measurements. The actual thickness of the spacer was measured to be 97  $\mu$ m. This was obtained with the interference fringes with the transmission cell filled with air, as shown in the SI Figure S3. For surface measurements, the SEIRAS spectra were backgrounded with respect to spectra of gold deposited on ZnSe in air, before their respective monolayers were assembled. We did not see any SEIRAS signal of 6-FCHT when the incident IR light was s polarized. Therefore, we took all the measurements with p polarized light. Note that this observation does not imply a perfectly ordered monolayer. The roughness of the gold surface implies that there are many orientations of the monolayer with respect to the polarization of light. However, as reported previously in the literature, the ppolarization sensitivity of SEIRAS arises from the response of the metal, rather than the orientation of the molecules.<sup>34</sup>

#### ■ RESULTS AND DISCUSSION

Surface Coverage of 6-FCHT Measured by Cyclic Voltammetry. Cyclic voltammograms of the SAM covered substrates were measured and the anodic/cathodic peaks were observed at +0.49 and +0.39 V vs Ag/AgCl, respectively, as shown in Figure 1. We note a peak-to-peak separation of 100

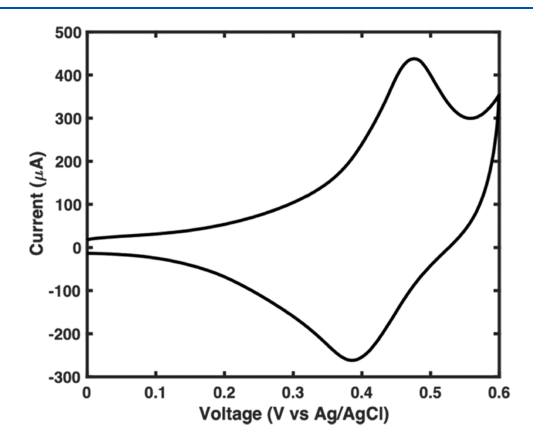


Figure 1. A representative cyclic voltammogram of the 6-FCHT monolayer at scan rate of 50~mV/s.

mV that deviates from that of the ideal surface-active voltammogram. This could be due to difference in the solvation of local environments that lead to a difference in the energetics for oxidizing and reducing the monolayer, as has been reported in the literature as well. We acknowledge a slight asymmetry between the anodic and cathodic peaks. However, if a polynomial background is subtracted, the difference between the integrated charge between the two peaks is not significant. We have shown the steps of the background and baseline subtractions, as well as the values for the cathodic and anodic integrations for a few representative CVs in the SI Figure S2. The surface coverage for a series of samples ranged between 0.122 and 1.86 molecules nm<sup>-2</sup> (see Table 1).

Molar Absorptivity of 6-FCHT Measured by Bulk FTIR. The bulk absorption spectra of 6-FCHT in the C-H stretch region as a function of various concentrations in dDMSO is shown in Figure 2. For determination of the bulk molar absorptivity of the hydrocarbon stretches of 6-FCHT, we used the peaks at 2853 and 2929 cm<sup>-1</sup>, which correspond to the symmetric and asymmetric CH2 stretches of the hydrocarbon chain. 40-43 The baseline corrected spectra and the absorbance values at 2853 and 2929 cm<sup>-1</sup> are plotted against the concentration of 6-FCHT as shown in Figure 2. The slope obtained from the absorbance verses concentration plot is the product of molar absorptivity and path length (97  $\mu$ m in our case). The molar absorptivity  $arepsilon_{
m bulk}$  of the symmetric and asymmetric stretches were found to be 71 and 126 M<sup>-1</sup> cm<sup>-1</sup>. The linear fits for the bulk absorption spectra showing the (0,0) point can be seen in the SI, Figure S4.

Enhancement Factor from SEIRAS. To calculate  $\varepsilon_{\rm SEIRAS}$ , we measured spectra of monolayers of 6-FCHT on the electrodes. The SEIRAS spectrum of the same sample from Figure 1 is shown in Figure 3. The two peaks at 2853 and 2929 cm<sup>-1</sup> match those observed in the bulk 6-FCHT spectrum.

Table 1. A Summary of the Four Samples of 6-FCHT Monolayers, Showing Surface Density, Adsorption for the Two C-H Stretch Nodes, and Their Retrieved Enhancement Factors

sample	$ ho$ (molecules/nm $^2$ )	$A_{\rm SEIRAS}$ (mOD)	f @ 2853 cm <sup>-1</sup>	$A_{ m SEIRAS}$ (mOD)	f @ 2929 cm <sup>-1</sup>
1	0.168	3.9	1968	6.1	1706
2	0.122	1.7	1181	4.5	1762
3	0.626	9.1	1232	14.2	1084
4	1.86	18.9	857	38.9	999
average			1310		1388
StDev			469		402

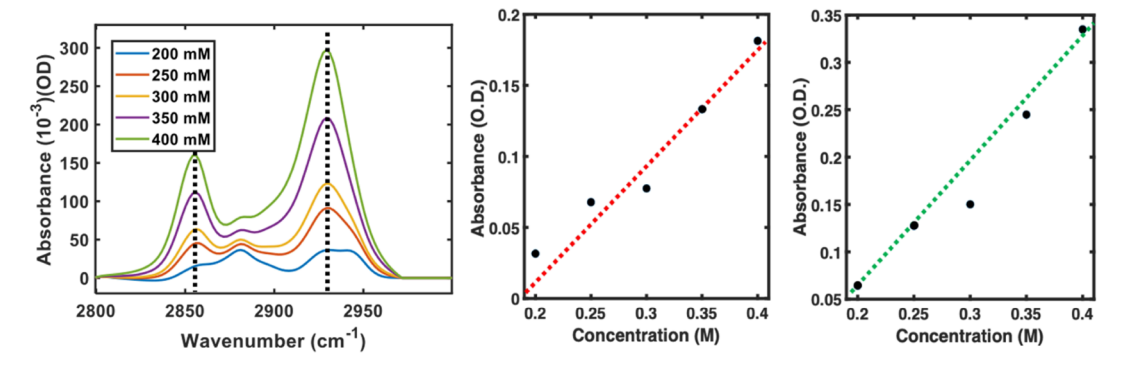
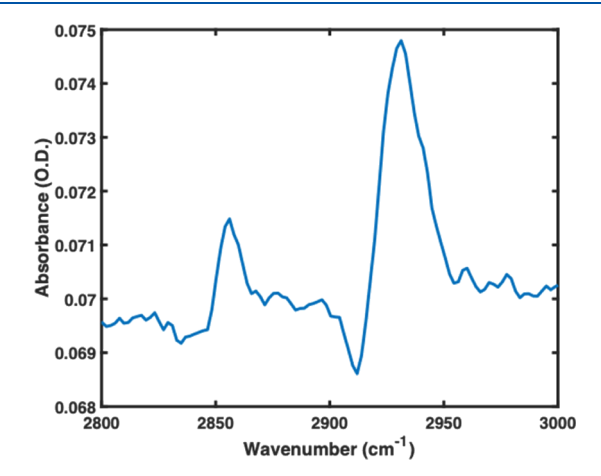


Figure 2. Bulk FTIR spectra corresponding to the C-H stretches of 6-FCHT. (a) The raw absorption of the C-H region as a function of 6-FCHT concentrations. (b) The peak heights of the 2853 cm<sup>-1</sup> and (c) 2929 cm<sup>-1</sup> peak plotted as function of 6-FCHT concentration.



**Figure 3.** SEIRAS spectrum of a 6-FCHT monolayer on gold in the C–H region. This is the same substrate used in Figure 1.

The absorption values at these same wavelengths were used for the calculation of the enhancement factors after the spectrum was background subtracted (SI Figure SS). The SEIRAS absorption based on an effective Beer's law for the surface is  $A_{\rm SEIRAS} = \varepsilon_{\rm SEIRAS} \ l \ c$ , where l and c are the effective path length and concentration. For a surface tethered species, the product of l and c is the surface density,  $\rho$ , leading to  $A_{\rm SEIRAS} = \varepsilon_{\rm SEIRAS} \ \rho$ . The enhancement factor f is defined as the ratio of the molar absorptivity of SEIRAS to that of the bulk  $f = \varepsilon_{\rm SEIRAS}/\varepsilon_{\rm bulk}$ . This leads to:

$$f = \frac{A_{\text{SEIRAS}}}{\rho \ \varepsilon_{\text{bulk}}}$$

Table 1 shows the enhancement factors for four different samples using the two SEIRAS absorption peaks at 2853 and 2929 cm<sup>-1</sup>. The average enhancement factor for the analysis at 2853 cm<sup>-1</sup> is  $1310 \pm 235$  and for 2929 cm<sup>-1</sup> is  $1360 \pm 201$ . In other words, the aliphatic C–H stretches of 6-FCHT is

enhanced by three orders of magnitude when it is close to the metal surface of a SEIRAS substrate.

We acknowledge that additional features exist in the C–H stretching region of the bulk FTIR spectra that do not manifest in the SEIRAS spectra. This could arise from spectral intensities that have been distributed differently due to conformational changes. This motivated us to perform another enhancement factor analysis using integration of all the C–H stretching peaks instead of the peak height absorption values at 2853 and 2929 cm $^{-1}$ . This can be seen in the SI Figure S6 and Table S1, where we extract an enhancement factor value of 762  $\pm$  82, which is in the same order of magnitude as the value calculated when the peak height absorption values were used.

It has been shown that organic groups with less than 16  $\rm CH_2$  groups form disordered layers.<sup>44</sup> Even if there was a perfect orientation of the molecules over the surface, the absorption coefficients would only change by a factor of 3. This is because isotropic averaging of a vector quantity (the transition dipole moment) results into introduction of a factor 1/3.45 Note that in the presence of roughened metal and in the limit of nearfield optics, the notion of polarization of the electromagnetic field can become complicated, and sometimes ill-defined. Furthermore, given the roughness of the gold substrate surfaces from the SEM images of our references, even if all the molecules preferentially adsorbed in one orientation, those orientations will still be randomized given the scale of roughness of the substrates being much larger than the scale of a single molecule adsorbed at the surface. Therefore, we do not consider the orientation of the monolayers in evaluating their interaction with light. Instead, we take the calculated enhancement factors as an averaged value over all orientations at the surface. Note that the enhancement factor retrieved based on the two peaks are quite close and within the error bars. It would be a nontrivial task to remove the chemisorbed monolayers after the calculation of the enhancement factor to reuse the substrates for another experiment. However, even though there is variability in the substrate preparation, they are

similar enough to give similar enhancement factors within errors presented in Table 1. Therefore, one can assume the substrates are comparable enough from one substrate to another, as long as they are prepared in similar conditions. We also note that unlike thermally deposited gold, these gold films are more robust. They can withstand multiple rounds of ultrasonication without flaking off or showing spectral changes, something that thermally deposited gold films could not do based on our previous experiences on Silicon and ITO. The explanation for the more robust substrate is because of a strong gold-selenium bond that forms upon deposition.<sup>31</sup>

Penetration Depth. Literature suggests that the surface enhancement is not uniformly distributed over the metal substrate, but rather arises from distinct "hot spots." 26,46,47 It is relatively straightforward to test this based on our estimated enhancement factor. We first assume that the enhancement factor of ~1000 is uniformly distributed across the metal film. Second, we assume that the enhancement decays exponentially into the solution. With these assumption in hand, we measured a spectrum of pure bulk acetonitrile above the SEIRAS substrate. Since we know the bulk molar absorptivity of acetonitrile, from the knowledge of SEIRAS absorption and enhancement factor, we can work out the penetration depth (see SI Figure S7). The retrieved penetration depth from this analysis is  $\sim$ 0.2 nm. This is non-physical since it is in the order of the length of a bond, and we know the IR light can penetrate through more than that from observation of spectral signatures of entities farther away. We also note that we do not believe the difference in enhancement factors between acetonitrile and Prussian blue stems from the difference in anisotropy. Furthermore, even if we account for anisotropy, it would introduce a change ~3 at most. In this case, the resulting penetration depth for acetonitrile would be ~0.6 nm, which is still unphysical. Therefore, the assumption of uniformly distributed enhancement factor is not valid. Rather, the measured ~1000 enhancement factor is an average over the entire surface where the hot spots necessarily have a much larger enhancement factor locally. Our experiment does not allow determination of the density of hot spots and the local enhancement factor. Therefore, our reported enhancement factor should be taken as an effective or averaged value.

Nonetheless, the question of effective penetration depth of the IR field into the sample remains. We resorted to another experiment to answer this question. We electrodeposited Prussian blue (PB) thin films on the SEIRAS substrate at increments of ~14 nm at a time while measuring the absorbance value of the nitrile stretches of PB. SI Figure S8 shows the calculation for the estimation of ~14 nm per deposition increment. As shown in Figure 4, the absorption signal of the Prussian Blue film continues to grow with the thickness of the film until it reaches a saturation point around 126 nm. From that point forward, the SEIRAS signal does not grow significantly while the electrodeposition continues as evidenced from Coulometry that shows current can still be sustained even after the SEIRAS signal stops growing. Since the method of electrodeposition relies on electron transfer from the electrode to cause the precipitation of the PB film and no other reactions can occur at this current, this means the film is still growing. A representative Coulometry is shown in SI Figure S8. This means that the penetration depth of the IR into the substrate was ~126 nm. Note that penetration depth of the IR field into the film is also a function of the thickness of the gold film, with thicker gold films resulting into smaller

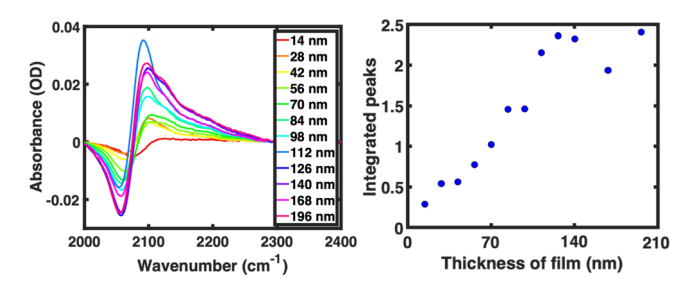


Figure 4. (Left) The SEIRAS spectrum of the PB film at different thicknesses and the (right) integrated peak area of the nitrile stretch of the PB film electrodeposited on the SEIRAS substrate  $\sim$ 14 nm increments.

penetration depths into the film (See SI Figure S10.). The penetration depth of the IR field into the sample is expected to be a function of the refractive index of the film. The refractive index of Prussian blue is reported to be  $\sim$ 1.44. Therefore, for materials and solvents of similar optical properties, a similar penetration depth is expected. Exact knowledge of the refractive index over a broad range frequency is quite rare, except for very common thin films used more broadly in industry. Additionally, the refractive index varies across an absorption. Many materials with strong visible absorptions, derive most of their IR refractive index from their response in the visible range. Often the absorption cross sections in the IR are much smaller than the visible cross sections, which is also true for Prussian blue as it is a vivid pigment in the visible range. Therefore, the dominant contribution will arise from the background refractive index as dictated by the response in the visible range, and not from the smaller absorption peaks in the IR range.

#### CONCLUSIONS

Knowledge of the plasmon enhancement factor for electrochemical ATR is necessary to elevate the observations of this technique from qualitative to quantitative. Here we presented a systematic approach which relies upon independent measurement of surface coverage, and yields enhancement factors in excess of 1000 for electroless deposited gold on ZnSe. Note that the enhancement factor will vary for different substrates and will depend on the metal. However, this method is generalizable and can be applied to other substrates and metals.

#### ASSOCIATED CONTENT

#### **Supporting Information**

The Supporting Information is available free of charge at https://pubs.acs.org/doi/10.1021/acs.langmuir.2c02254.

Electrochemical behavior of substrates; capacitive current background subtraction of cyclic voltammogram; interference fringe pattern of bulk FTIR cell; linear fits for bulk FTIR measurements; representative background subtracted SEIRAS spectrum; bulk FTIR spectra; enhancement factor using spectra integration method; penetration depth calculation; Prussian blue electrodeposition calculation and chronoamperometry; Prussian blue penetration depth (PDF)

#### AUTHOR INFORMATION

#### **Corresponding Author**

Jahan M. Dawlaty — Department of Chemistry, University of Southern California, California, Los Angeles 90089, United States; © orcid.org/0000-0001-5218-847X;

Email: dawlaty@usc.edu

#### **Authors**

Cindy Tseng – Department of Chemistry, University of Southern California, California, Los Angeles 90089, United States

Anuj K. Pennathur – Department of Chemistry, University of Southern California, California, Los Angeles 90089, United States

Drew Blauth – Department of Chemistry, Lewis & Clark College, Portland, Oregon 97219, United States Noemi Salazar – Department of Chemistry, The Ohio State University, Columbus, Ohio 43210, United States

Complete contact information is available at: https://pubs.acs.org/10.1021/acs.langmuir.2c02254

#### **Funding**

This work was supported by the Air Force Office of Scientific Research under AFOSR award FA9550-18-1-0420. CT was partially supported by the Anton B. Burg Foundation teaching award.

#### **Notes**

The authors declare no competing financial interest.

#### REFERENCES

- (1) Hartstein, A.; Kirtley, J.; Tsang, J. Enhancement of the infrared absorption from molecular monolayers with thin metal overlayers. *Phys. Rev. Lett.* **1980**, *45*, 201.
- (2) Corson, E. R.; Kas, R.; Kostecki, R.; Urban, J. J.; Smith, W. A.; McCloskey, B. D.; Kortlever, R. In Situ ATR-SEIRAS of Carbon Dioxide Reduction at a Plasmonic Silver Cathode. *J. Am. Chem. Soc.* **2020**, *142*, 11750–11762.
- (3) Deng, W.; Zhang, L.; Dong, H.; Chang, X.; Wang, T.; Gong, J. Achieving convenient CO 2 electroreduction and photovoltage in tandem using potential-insensitive disordered Ag nanoparticles. *Chem. Sci.* **2018**, *9*, 6599–6604.
- (4) Wuttig, A.; Liu, C.; Peng, Q.; Yaguchi, M.; Hendon, C. H.; Motobayashi, K.; Ye, S.; Osawa, M.; Surendranath, Y. Tracking a Common Surface-Bound Intermediate during CO2-to-Fuels Catalysis. *ACS Cent. Sci.* **2016**, *2*, 522–528.
- (5) Kas, R.; Ayemoba, O.; Firet, N. J.; Middelkoop, J.; Smith, W. A.; Cuesta, A. In-Situ Infrared Spectroscopy Applied to the Study of the Electrocatalytic Reduction of CO2: Theory, Practice and Challenges. *ChemPhysChem* **2019**, *20*, 2904–2925.
- (6) Ge, W.; Chen, Y.; Fan, Y.; Zhu, Y.; Liu, H.; Song, L.; Liu, Z.; Lian, C.; Jiang, H.; Li, C. Dynamically Formed Surfactant Assembly at the Electrified Electrode—Electrolyte Interface Boosting CO2 Electroreduction. *J. Am. Chem. Soc.* **2022**, *144*, 6613–6622.
- (7) Wuttig, A.; Ryu, J.; Surendranath, Y. Electrolyte competition controls surface binding of CO intermediates to CO2 reduction catalysts. *J. Phys. Chem. C* **2021**, *125*, 17042–17050.
- (8) Wuttig, A.; Yaguchi, M.; Motobayashi, K.; Osawa, M.; Surendranath, Y. Inhibited proton transfer enhances Au-catalyzed CO2-to-fuels selectivity. *Proc. Natl. Acad. Sci. U. S. A.* **2016**, *113*, E4585–E4593.
- (9) Ovalle, V. J.; Hsu, Y.-S.; Agrawal, N.; Janik, M. J.; Waegele, M. M. Correlating hydration free energy and specific adsorption of alkali metal cations during CO2 electroreduction on Au. *Nat. Catal.* **2022**, *5*, 624–632.

- (10) Li, J.; Li, X.; Gunathunge, C. M.; Waegele, M. M. Hydrogen bonding steers the product selectivity of electrocatalytic CO reduction. *Proc. Natl. Acad. Sci. U. S. A.* **2019**, *116*, 9220–9229.
- (11) Yeh, P.-H.; Venkatesan, S.; Chen, H.-C.; Lee, Y.-L. In-Situ surface enhanced infrared absorption spectroscopy study of electrocatalytic oxidation of ethanol on Platinum/Gold surface. *Spectrochim. Acta, Part A* **2022**, *271*, No. 120902.
- (12) Yang, Y.-Y.; Ren, J.; Zhang, H.-X.; Zhou, Z.-Y.; Sun, S.-G.; Cai, W.-B. Infrared spectroelectrochemical study of dissociation and oxidation of methanol at a palladium electrode in alkaline solution. *Langmuir* **2013**, *29*, 1709–1716.
- (13) Zhu, C.; Lan, B.; Wei, R.-L.; Wang, C.-N.; Yang, Y.-Y. Potential-dependent selectivity of ethanol complete oxidation on Rh electrode in alkaline media: a synergistic study of electrochemical ATR-SEIRAS and IRAS. ACS Catal. 2019, 9, 4046–4053.
- (14) Yoshida, M.; Yamakata, A.; Takanabe, K.; Kubota, J.; Osawa, M.; Domen, K. ATR-SEIRAS Investigation of the Fermi Level of Pt Cocatalyst on a GaN Photocatalyst for Hydrogen Evolution under Irradiation. J. Am. Chem. Soc. 2009, 131, 13218–13219.
- (15) Oliveira, N. J.; Xu, B.; Yan, Y. Evidence for the Lack of Caffeine Specific Adsorption and Its Impact on Water Structure to Increase HOR/HER Activity on Pt, ECS Meeting Abstracts; IOP Publishing: 2021; p. 1484
- (16) Kunimatsu, K.; Senzaki, T.; Tsushima, M.; Osawa, M. Reaction intermediate of hydrogen evolution reaction on a Pt electrode studied by surface-enhanced infrared spectroscopy. In 206th Meeting of the Electrochemical Society, Honolulu, HI, USA, 2004.
- (17) Zhang, Z.-Q.; Banerjee, S.; Thoi, V. S.; Shoji Hall, A. Reorganization of Interfacial Water by an Amphiphilic Cationic Surfactant Promotes CO2 Reduction. *J. Phys. Chem. Lett.* **2020**, *11*, 5457–5463.
- (18) Li, S.; Wu, L.; Zhang, X.; Jiang, X. The structure of water bonded to phosphate groups at the electrified zwitterionic phospholipid membranes/aqueous interface. *Angew. Chem. Int. Ed.* **2020**, *59*, 6627–6630.
- (19) Grossutti, M.; Leitch, J. J.; Seenath, R.; Karaskiewicz, M.; Lipkowski, J. SEIRAS studies of water structure in a sodium dodecyl sulfate film adsorbed at a gold electrode surface. *Langmuir* **2015**, *31*, 4411–4418.
- (20) Burdach, K.; Dziubak, D.; Sek, S. Surface-Enhanced Infrared Absorption Spectroscopy (SEIRAS) to Probe Interfacial Water in Floating Bilayer Lipid Membranes (fBLMs). In *Membrane Lipids*; Springer: 2022; pp. 199–207.
- (21) Woods, D. A.; Bain, C. D. Total internal reflection spectroscopy for studying soft matter. *Soft Matter* **2014**, *10*, 1071–1096.
- (22) Sun, D.-W. Infrared spectroscopy for food quality analysis and control; Academic press: 2009.
- (23) Osawa, M. Surface-enhanced infrared absorption. In Near-field optics and surface plasmon polaritons; Springer: 2001; pp. 163–187.
- (24) Andvaag, I. R.; Morhart, T. A.; Clarke, O. J. R.; Burgess, I. J. Hybrid Gold—Conductive Metal Oxide Films for Attenuated Total Reflectance Surface Enhanced Infrared Absorption Spectroscopy. *ACS Appl. Nano Mater.* **2019**, *2*, 1274—1284.
- (25) Killian, M. M.; Villa-Aleman, E.; Sun, Z.; Crittenden, S.; Leverette, C. L. Dependence of surface-enhanced infrared absorption (SEIRA) enhancement and spectral quality on the choice of underlying substrate: A closer look at silver (Ag) films prepared by physical vapor deposition (PVD). *Appl. Spectrosc.* **2011**, *65*, 272–283.
- (26) Wang, H.-L.; You, E.-M.; Panneerselvam, R.; Ding, S.-Y.; Tian, Z.-Q. Advances of surface-enhanced Raman and IR spectroscopies: from nano/microstructures to macro-optical design. *Light* **2021**, *10*, 161.
- (27) Leverette, C.; Jacobs, S.; Shanmukh, S.; Chaney, S.; Dluhy, R.; Zhao, Y.-P. Aligned silver nanorod arrays as substrates for surface-enhanced infrared absorption spectroscopy. *Appl. Spectrosc.* **2006**, *60*, 906–913.
- (28) Brown, L. V.; Zhao, K.; King, N.; Sobhani, H.; Nordlander, P.; Halas, N. J. Surface-enhanced infrared absorption using individual

- cross antennas tailored to chemical moieties. J. Am. Chem. Soc. 2013, 135, 3688-3695.
- (29) Ataka, K.; Stripp, S. T.; Heberle, J. Surface-enhanced infrared absorption spectroscopy (SEIRAS) to probe monolayers of membrane proteins. *Biochim. Biophys. Acta* **2013**, *1828*, 2283–2293.
- (30) Kawata, S.; Ohtsu, M.; Irie, M. Near-field optics and surface plasmon polaritons; Springer Science & Business Media: 2001; Vol. 81.
- (31) Bao, W.-J.; Li, J.; Li, J.; Zhang, Q.-W.; Liu, Y.; Shi, C.-F.; Xia, X.-H. Au/ZnSe-based surface enhanced infrared absorption spectroscopy as a universal platform for bioanalysis. *Anal. Chem.* **2018**, *90*, 3842–3848.
- (32) Elgrishi, N.; Rountree, K. J.; McCarthy, B. D.; Rountree, E. S.; Eisenhart, T. T.; Dempsey, J. L. A Practical Beginner's Guide to Cyclic Voltammetry. *J. Chem. Educ.* **2018**, *95*, 197–206.
- (33) Roig, A.; Navarro, J.; Garcia, J.; Vicente, F. Voltammetric study of the stability of deposited Prussian blue films against succesive potential cycling. *Electrochim. Acta* **1994**, *39*, 437–442.
- (34) Osawa, M.; Ataka, K.-I.; Yoshii, K.; Nishikawa, Y. Surface-enhanced infrared spectroscopy: the origin of the absorption enhancement and band selection rule in the infrared spectra of molecules adsorbed on fine metal particles. *Appl. Spectrosc.* **1993**, 47, 1497–1502.
- (35) Murray, R. W. Chemically modified electrodes. *Acc. Chem. Res.* 1980, 13, 135–141.
- (36) Smalley, J. F.; Finklea, H. O.; Chidsey, C. E.; Linford, M. R.; Creager, S. E.; Ferraris, J. P.; Chalfant, K.; Zawodzinsk, T.; Feldberg, S. W.; Newton, M. D. Heterogeneous electron-transfer kinetics for ruthenium and ferrocene redox moieties through alkanethiol monolayers on gold. *J. Am. Chem. Soc.* 2003, 125, 2004–2013.
- (37) Dionne, E. R.; Badia, A. Electroactive self-assembled monolayers detect micelle formation. ACS Appl. Mater. Interfaces 2017, 9, 5607–5621.
- (38) Nguyen, K.-L.; Dionne, E. R.; Badia, A. Redox-controlled ion-pairing association of anionic surfactant to ferrocene-terminated self-assembled monolayers. *Langmuir* **2015**, *31*, 6385–6394.
- (39) Peng, Z.; Qu, X.; Dong, S. Co-assembly of ferrocene-terminated and alkylthiophene thiols on gold and its redox chemistry modulated by surfactant adsorption. *J. Electroanal. Chem.* **2004**, *563*, 291–298.
- (40) Sung, W.; Kim, D.; Shen, Y. Sum-frequency vibrational spectroscopic studies of Langmuir monolayers. *Curr. Appl. Phys.* **2013**, 13, 619–632.
- (41) Vail, T. L.; Cushing, K. W.; Ingram, J. C.; Omer, I. S. Micropatterned avidin arrays on silicon substrates via photo-lithography, self-assembly and bioconjugation. *Biotechnol. Appl. Biochem.* **2006**, 43, 85–91.
- (42) Yu, P. Detect Structure Features of Asymmetric and Symmetric CH2 and CH3 Functional Groups and Their Ratio of Biopolymers within Intact Tissue in Complex Plant System Using Synchrotron FTIRM and DRIFT Molecular Spectroscopy. In *Biopolymers*; IntechOpen: 2010.
- (43) Lu, R.; Gan, W.; Wu, B.-h.; Chen, H.; Wang, H.-f. Vibrational polarization spectroscopy of CH stretching modes of the methylene group at the vapor/liquid interfaces with sum frequency generation. *J. Phys. Chem. B* **2004**, *108*, 7297–7306.
- (44) Smiley, B.; Richmond, G. Alkyl Chain Ordering of Asymmetric Phosphatidylcholines Adsorbed at a Liquid Liquid Interface. *J. Phys. Chem. B* **1999**, *103*, 653–659.
- (45) Andrews, S. S. Using rotational averaging to calculate the bulk response of isotropic and anisotropic samples from molecular parameters. *J. Chem. Educ.* **2004**, *81*, 877.
- (46) Eid, S. M.; Hassan, S. A.; Nashat, N. W.; Elghobashy, M. R.; Abbas, S. S.; Moustafa, A. A. Optimization of localized surface plasmon resonance hot spots in surface-enhanced infrared absorption spectroscopy aluminum substrate as an optical sensor coupled to chemometric tools for the purity assay of quinary mixtures. *Microchim. Acta* 2021, 188, 195.
- (47) Le, F.; Brandl, D. W.; Urzhumov, Y. A.; Wang, H.; Kundu, J.; Halas, N. J.; Aizpurua, J.; Nordlander, P. Metallic Nanoparticle Arrays: A Common Substrate for Both Surface-Enhanced Raman

Scattering and Surface-Enhanced Infrared Absorption. ACS Nano 2008, 2, 707–718.

(48) Ngo, G.; Félix, G.; Long, J.; Costa, L.; Saavedra, O.; Milhiet, P.-E.; Devoisselle, J.-M.; Guari, Y.; Larionova, J.; Chopineau, J. A simple approach for controlled deposition of Prussian blue analogue nanoparticles on a functionalised plasmonic gold surface. *New J. Chem.* **2019**, 43, 3660–3664.

### **□** Recommended by ACS

Quantitatively Revealing the Anomalous Enhancement in Shell-Isolated Nanoparticle-Enhanced Raman Spectroscopy Using Single-Nanoparticle Spectroscopy

Shu Hu, Jian-Feng Li, et al.

DECEMBER 05, 2022

ACS NANO

Toward Quantitative Surface-Enhanced Raman Scattering with Plasmonic Nanoparticles: Multiscale View on Heterogeneities in Particle Morphology, Surface Modifica...

Jiwoong Son, Jwa-Min Nam, et al.

DECEMBER 06, 2022

JOURNAL OF THE AMERICAN CHEMICAL SOCIETY

READ 🗹

READ **C** 

## Ionic-Wind-Enhanced Raman Spectroscopy without Enhancement Substrates

Qingyou Liang, Guangzhao Zhang, et al.

DECEMBER 28, 2022

ANALYTICAL CHEMISTRY

READ **C** 

#### Chemical Interface Damping-Induced Attenuation of Surface Plasmon-Enhanced Raman Spectroscopy

Shuyi Zhu, Weiping Cai, et al.

SEPTEMBER 09, 2022

ACS PHOTONICS

READ 🗹

Get More Suggestions >